

A compressed data approach for image-domain least-squares migration

Ram Tuvi¹, Zeyu Zhao¹, and Mrinal Kanti Sen¹

ABSTRACT

We consider the problem of image-domain least-squares migration (LSM) based on efficiently constructing the Hessian matrix with sparse beam data. Specifically, we use the ultra-wide-band phase space beam summation method, in which beams are used as local basis functions to represent scattered data collected at the surface. The beam domain data are sparse. One can identify seismic events with significant contributions so that only beams with nonnegligible amplitudes need to be used to image the subsurface. In addition, due to the beams' spectral localization, only beams that pass near an imaging point need to be taken into account. These two properties reduce the computational complexity of computing the Hessian matrix - an essential ingredient for LSM. As a result, we can efficiently construct the Hessian matrix based on analyzing the sparse beam domain data.

INTRODUCTION

Seismic migration methods are able to obtain subsurface images from surface data (Claerbout, 1976). Because migration is an adjoint operator, obtained images contain errors due to the limited data, background model, and noise. Tarantola (1984) and Schuster (1993) suggest formulating the migration problem as a least-squares inversion method by minimizing the difference between observed and predicted data. These formulations are known as least-squares migration (LSM). Compared to a migrated image, LSM improves the image resolution, reduces migration noise, and balances the amplitude for poorly and well-illuminated regions.

LSM formulations are implemented in either the data domain (Schuster, 1993; Nemeth et al., 1999; Dai et al., 2012) or the image domain (Plessix, 2006; Yu et al., 2006; Aoki and Schuster, 2009). The former uses iterative schemes to minimize the misfit between the predicted and observed data. In general, data-domain formulations require solving the wave equation at each iteration, which hampers computational efficiency. Image-domain formulations are based on constructing and inverting a Hessian matrix. However, constructing and inverting the Hessian matrix can be computationally expensive for large physical models. Different approximations to the Hessian matrix have been studied by Plessix (2006), Valenciano et al. (2006), Yu et al. (2006), Tang (2009), and Aoki and Schuster (2009). These approaches show a great reduction in computational complexity without significantly impairing image quality.

Beam summation methods provide an accurate and efficient tool in seismic wave propagation (Červený, 1982). The main advantage of these formulations comes from the spectral locality of the beams. When propagating the field, only beams passing near an imaging point should be considered. Hill (2001) suggests a migration approach based on expanding the source and receiver Green's functions (GFs) as a sum of beams resulting in an efficient tool to obtain a high-resolution image. Based on these advantages, several beam-based LSM approaches have been proposed, with efficient Hessian approximations (Hu et al., 2016; Yuan et al., 2017; Yue et al., 2021).

In this work, we adopt the migration formulations of Tuvi et al. (2020a, 2020b) to efficiently construct the full Hessian matrix. These approaches are based on the ultra-wide-band phase space beam summation (UWB-PS-BS) method (Shlivinski et al., 2004), which uses windowed Fourier transform (WFT) frame decomposition of surface fields. The WFT migration approach is different from traditional Gaussian beam (GB) migration methods based on localized source expansions. With WFT, the original shot gathers are transformed into the beam domain rather than the shot-receiver gathers used in traditional GB methods. Then, the migration is performed by constructing the beam propagators and imaging the corresponding beam data, which represent the beam to beam scattering amplitudes. Thus, the imaging task is completely formulated in the beam domain. Detailed comparisons between the traditional GB and WFT methods can be found in Tuvi et al. (2020b). Under the Born approximation, the beam data are directly related to spe-

Manuscript received by the Editor 21 March 2021; revised manuscript received 6 May 2021; published ahead of production 15 July 2021; published online 7

September 2021.

The University of Texas at Austin, Institute for Geophysics, John A. and Katherine G. Jackson School of Geosciences, Austin, Texas 78758, USA. E-mail: ram@ig.utexas.edu (corresponding author); zeyu@utexas.edu; mrinal@utexas.edu.

© 2021 Society of Exploration Geophysicists. All rights reserved.

A52 Tuvi et al.

cific scatterers over the subsurface. When implementing LSM, only beams with significant amplitude need to be used to construct the propagation operator, the migrated image, and the Hessian matrix. Because the data transformation is performed before migration, one can filter out less relevant data for imaging. This thresholding operation adds an a priori degree of localization to the LSM problem. Compared with traditional GB methods, the new formulation makes it easier to analyze the data prior to migration and the imaging process is much more flexible. Combining this unique property with the beams' spectral locality significantly reduces the computational complexity of the image-domain LSM problem.

BEAM-BASED MIGRATION

The proposed LSM method is based on the migration algorithm of Tuvi et al. (2020b). One uses WFT frames with GBs to expand the data and backpropagate the fields. This theory is based on the UWB-PS-BS method presented by Shlivinski et al. (2004). The frame elements are

$$\hat{\psi}_{\mu} = \hat{\psi}(\mathbf{x} - \mathbf{x}_{\mathbf{m}})e^{-i\omega\mathbf{p}_{\mathbf{n}}\cdot(\mathbf{x} - \mathbf{x}_{\mathbf{m}})}, \quad \mu = (\mathbf{m}, \mathbf{n}) = ((m_1, m_2), (n_1, n_2)),$$
(1)

with $\hat{\psi}$ being a window function. Henceforth, the over-caret denotes the frequency-dependent quantities. The index μ that tags the frame elements defines a spatial (x)-spectral (p) phase-space lattice via $\mathbf{x}_{\mathbf{m}} = \mathbf{m}\bar{x}$, $\mathbf{p}_{\mathbf{n}} = \mathbf{n}\bar{p}$, with \bar{x} and \bar{p} being the unit cell dimensions, at each direction over this lattice. Each element is localized around points $\mathbf{x}_{\mathbf{m}}$ and $\mathbf{p}_{\mathbf{n}}$ over the x and p directions, respectively (Tuvi et al., 2020b, Figure 1).

The frame should be overcomplete; i.e., the unit cell area should satisfy $\omega \bar{x} \, \bar{p} < 2\pi \nu$, with $\nu < 1$ being the overcompleteness parameter. We also define a dual frame set $\{\hat{\varphi}_{\mu}(\mathbf{x})\}$ used to expand the data. In general, $\hat{\varphi}$ should be calculated numerically. However, if the frame is highly overcomplete $(\nu < 0.3)$, it can be approximated analytically via $\hat{\varphi} \approx (\nu/\|\hat{\psi}(\mathbf{x})\|)^2 \hat{\psi}(\mathbf{x})$ (Shlivinski et al., 2004). Typically, $\hat{\psi}$ is chosen to be a Gaussian window. This choice leads to a snug frame for all frequencies in the band, leading to localized and stable dual frame functions and expansion coefficients. Hill (2001) obtains similar overcompleteness criteria via the oversampling theorem.

We denote by $\hat{\mathbf{d}}(\mathbf{x}_s, \mathbf{x}_r)$ the data collected at the receiver located at $\mathbf{x} = \mathbf{x}_r$ due to a point source located at $\mathbf{x} = \mathbf{x}_s$. The beam representation of the data $\hat{A}_{\mu,\mu'}$ is given by Tuvi et al. (2020b) as

$$\hat{A}_{\mu,\mu'} = \int d^2x_s \hat{\varphi}_{\mu}(\mathbf{x_s}) \int d^2x_r \hat{\varphi}_{\mu'}^*(\mathbf{x_r}) \hat{\mathbf{d}}(\mathbf{x_r}, \mathbf{x_s}), \quad (2)$$

with μ and μ' being the source and receiver beams, respectively, whereas the asterisk denotes the complex conjugate. The corresponding migrated image is given by

$$\mathbf{m}_{\text{mig}}(\mathbf{r}) = \text{Re} \int_0^\infty d\omega \omega^2 \hat{f}^* \sum_{\mu,\mu'} \hat{\Lambda}_{\mu,\mu'}(\mathbf{r}) \hat{A}_{\mu,\mu'}, \qquad (3)$$

with \hat{f} being the frequency spectrum of the source. The functions $\hat{\Lambda}_{\mu,\mu'}(\mathbf{r}) = \hat{\Psi}^*_{\mu}(\mathbf{r})\hat{\Psi}^b_{\mu'}(\mathbf{r})$ are the imaging kernels, which can be obtained by multiplying a pair of source and receiver (backpropagated) beams, respectively.

APPLICATION FOR IMAGE-DOMAIN LSM

Under the Born approximation, the shot gathers are related to the reflectivity of the model $\mathbf{m_r}$ via the propagation operator $\hat{\mathbf{L}}$:

$$\hat{\mathbf{d}}(\mathbf{x}_{\mathbf{r}}, \mathbf{x}_{\mathbf{s}}) \simeq \hat{\mathbf{L}}\mathbf{m}_{\mathbf{r}}, \qquad \hat{\mathbf{L}} = \omega^2 \hat{f} \hat{G}_B(\mathbf{r}, \mathbf{x}_{\mathbf{s}}) \hat{G}_B(\mathbf{r}, \mathbf{x}_{\mathbf{r}}), \quad (4)$$

with \hat{G}_B being the background GF. Introduction of equation 2 into equation 4, and using the frame relation above, the Born approximation of the scattered beam data is given by

$$\hat{\mathbf{A}}_{\mu,\mu'} = \frac{\nu^4}{\|\hat{\boldsymbol{\psi}}(\mathbf{x})\|^4} \hat{\mathbf{L}}_{\mu,\mu'} \mathbf{m}_{\mathbf{r}},\tag{5}$$

with $\hat{\mathbf{L}}_{\mu,\mu'} = f(\omega)\omega^2\hat{\mathbf{\Lambda}}_{\mu,\mu'}^*$ being the beam propagation operator. The estimated reflectivity can be written as

$$\mathbf{m_r} = (\hat{\mathbf{L}}_{\mu,\mu}^{\dagger} \hat{\mathbf{L}}_{\mu,\mu})^{-1} \hat{\mathbf{L}}_{\mu,\mu'}^{\dagger} \frac{\hat{\mathbf{A}}_{\mu,\mu'} \|\hat{\boldsymbol{\psi}}(\mathbf{x})\|^4}{\nu^4}, \tag{6}$$

with \dagger being the adjoint operator. Equation 5 represents the beam data as the interaction between the imaging kernels and the medium reflectivity, whereas the operation in equation 6 expresses the estimated reflectivity as the inverse Hessian matrix $(\hat{\mathbf{L}}_{\mu,\mu'}^{\dagger}\hat{\mathbf{L}}_{\mu,\mu'})^{-1}$ applied on the migrated image of equation 3. Constructing the full Hessian matrix is computationally expensive due to the model size. In addition, a large number of crosscorrelation operations between the sources and receivers are needed to obtain the Hessian matrix elements. Here, we use a compressed data set to efficiently construct the Hessian matrix.

Under the Born approximation, the beam domain data can be interpreted as applying the propagation operator $\hat{\mathbf{L}}_{\mu,\mu'}$ on the medium reflectivity m_r. As noted by Tuvi et al. (2020b), the corresponding data are governed by the subsurface reflection obtained from localized areas and in specific directions (local Snell's law reflection). The migrated image of equation 3 is obtained by applying the propagation operator on the beam domain data. Using the local Snell's law interpretation of the data, we can filter out low-amplitude data. Thus, we can compress the data size needed for imaging and threshold the corresponding imaging kernels in the propagation operator. The imaging kernels are obtained by multiplying two beam propagators. Each beam propagates along its axis and decays from it. Given an imaging point, only pairs of beams that overlap there will contribute to the image. As a result, the beam propagation operator can be represented using only a subset of imaging kernels. This compressed representation is based on physical properties of the subsurface. Because the data transformation is calculated over the surface before constructing the image, the proposed formulation can a priori reduce the number of calculations needed to construct the Hessian matrix.

NUMERICAL EXAMPLE

We demonstrate our LSM algorithm via the Marmousi model. The model comprises 460 and 150 points in the distance and depth directions, respectively, with a 0.02 km grid spacing in both directions. To reduce memory costs, we use 0.04 km grid for imaging. The reflectivity model is shown in Figure 1a. We use the frequency range f = [5, 25] Hz for imaging, with the frequency interval of $\Delta f = 0.25$ Hz. We set the beam parameter b = 20, and we obtain

16 beam initiation points, with the 43 initial propagation directions with a spectral range $p_n = [-0.42, 0.42]$ s/km and unit cell dimensions $\bar{x} \approx 0.6$ km, $\bar{p} \approx 0.03$ s/km (Tuvi et al., 2020b, equation 13). This choice of b leads to collimated beams for all of the propagation domain, whereas the beams' width is defined as described in Hill (2001). The beam propagators are calculated via numerical integration with background GFs (Tuvi et al., 2020b, equation 9). These GFs are uniformly distributed over the surface with $\Delta x = 0.02$ km spacing and calculated by solving the frequency-domain acoustic wave equation. Using these beam propagators, we calculate Born modeling data corresponding to equation 5.

In Figure 1b, we plot the full data set of equation 5, at the frequency f = 10 Hz normalized to their maximal value at this

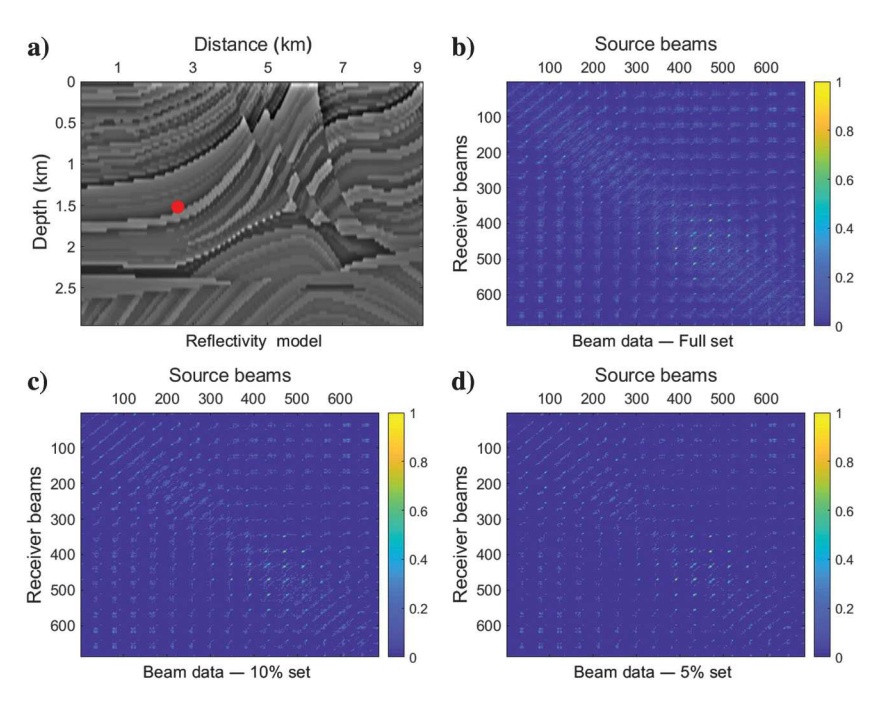


Figure 1. The reflectivity model and the beam representation of the shot gathers. (a) Reflectivity and (b-d) beam data of equation 5 for frequency f = 10 Hz, normalized to their maximal value at this frequency, obtained by the full, 10%, and 5% of the highest amplitudes, respectively. The size of the axes is the number of source and receiver beams. The full data are sparse. Thus, we may use only the sparse data set as (c and d).

frequency. The axes are in the size of source and receiver beams, where we arrange them as concatenated vectors with each beam initiation point and all propagation directions. Each point over this grid represents an imaging kernel amplitude (beam-to-beam scattering amplitude). The data are sparse. Following the preceding discussion, the amplitudes correspond to scattering events over the subsurface. In Figure 1c and 1d, we plot the data at the same frequency for the top 10% and 5%, respectively, of the highest amplitudes. Major subsurface scattering energy is still kept in the thresholded sparse sets. One may use only high-amplitude imaging kernels for imaging. Only these imaging kernels contain significant energy needed to construct the image.

To explore the sparse Hessian matrix structure, we plot in

Figure 2a-2c a row of the Hessian matrices calculated using the full data set, 10%, and 5% of the full data set at the point $\mathbf{r} = (2.6, 1.52)$ km, highlighted by the red dot in Figure 1a. To obtain the sparse Hessian, we threshold the data with the top highest amplitudes at each frequency. Only the corresponding imaging kernels are used to construct the Hessian. The beam data near this area correspond to the angle between the incident and backpropagated beams. The data also correspond to the reflector angle near this point. The full data set Hessian in Figure 2a is localized around the imaging point. The Hessian matrices calculated from the sparse data sets still extract the correlation information between the imaging point and its neighborhood points, although not as accurately as the full data set Hessian.

Constructing the full Hessian with the full data set requires 500,000 crosscorrelations at each frequency, which is too computationally costly on a desktop machine. For this reason, we only provide the number of crosscorrelations instead of the absolute computing time. With 10% and 5% of the full data set, only 50,000 and 25,000 crosscorrelations are required, respectively, at each frequency and can be performed directly on a desktop machine. With the sparse data, we greatly reduce the number of crosscorrelations, which significantly reduces the computational complexity.

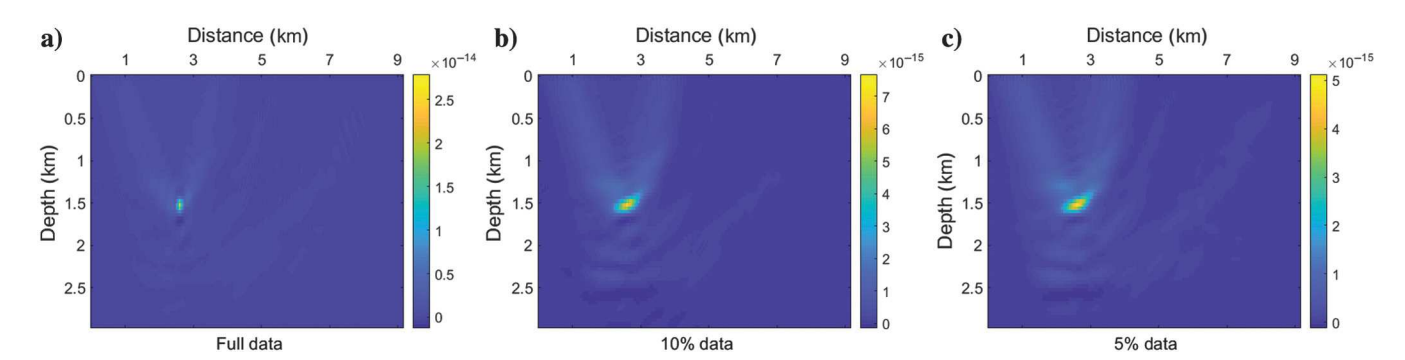


Figure 2. Hessian row corresponding to the point $\mathbf{r} = (2.6, 1.52)$ km calculated by the full and sparse data sets. (a) Full data, (b) 10% of the highest amplitude data, and (c) 5% of the highest amplitude data.

A54 Tuvi et al.

In Figure 3a–3c, we plot the images obtained by the beam-based migration operation of Tuvi et al. (2020b) for the full, 10%, and 5% sparse data sets, respectively, whereas in Figure 3d–3f, we plot the LSM images obtained by the proposed method. Applying the inverse of the Hessian to the migration image is achieved by an iterative conjugate gradient method. The image quality is significantly improved by the proposed LSM method compared to the migration results. We reconstruct most of the subsurface structures while substantially reducing the computational cost by approximating the Hessian with a small number of terms. In Figure 3g–3i, we compare the LSM results with the true reflectivity model at x = 4.6 km. The LSM results all resemble the true values. Then, we implement the algorithm using more realistic full wavefield data, generated using the time-domain rapid expansion method (Pestana and Stoffa, 2010). The physical

configuration is the same as previously. The migration and LSM images are plotted in Figure 4a–4c and 4d–4f, respectively. Compared to the migration image, the LSM results have better resolution with improved energy balance for all events, especially for poorly illuminated regions. Because the data used in these tests are full wavefield data that do not fully obey the Born approximation, we do note slightly worse image qualities compared with the LSM results obtained using the Born data, where the same engine is used for modeling and imaging. We reconstruct most of the subsurface even with 5% of the data, which significantly reduces the computational cost. These results agree with our physical model. They also demonstrate the advantage of the phase-space data representation because it filters only the relevant data needed for imaging. Therefore, only a few beams are needed to image the subsurface.

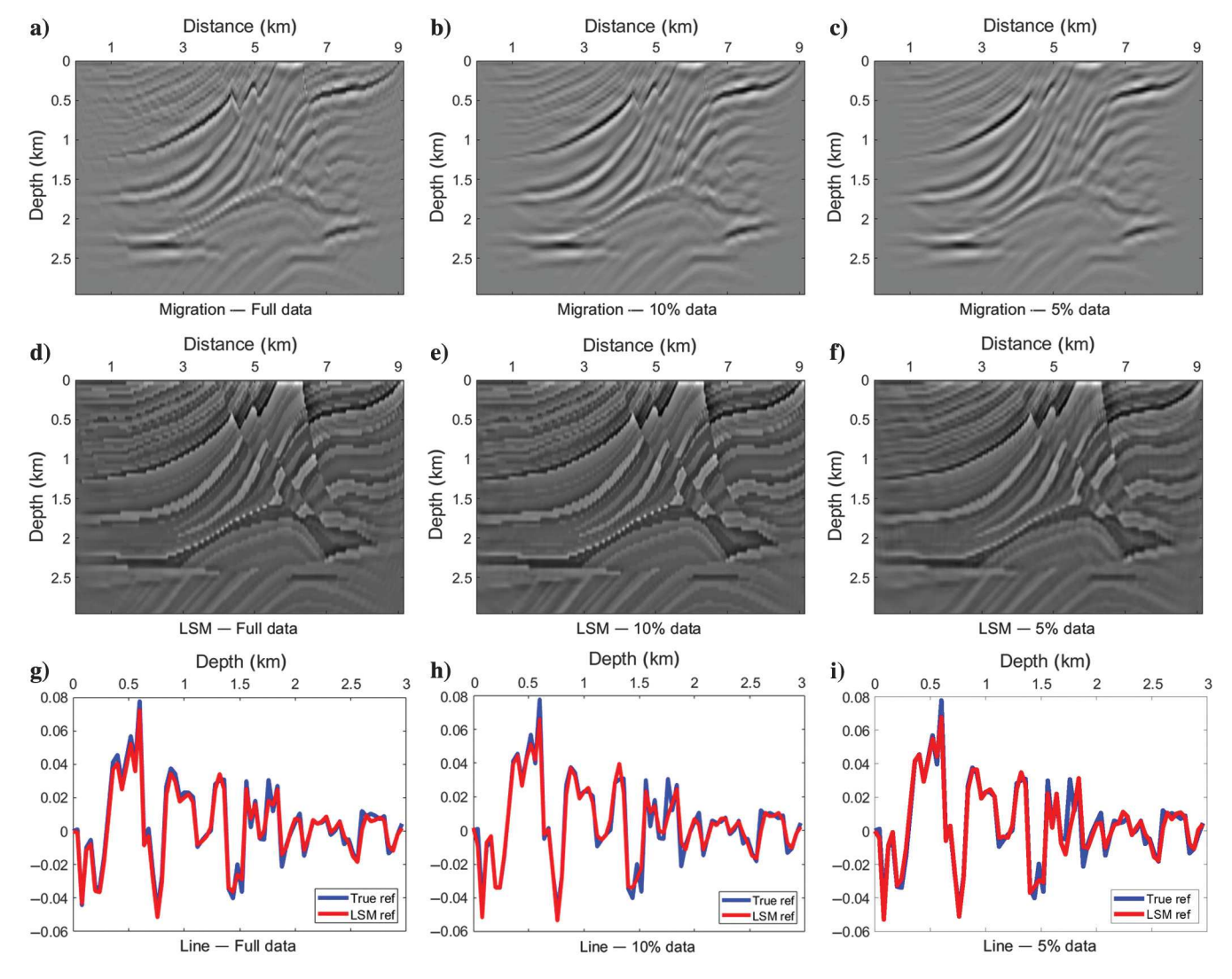


Figure 3. Image results obtained by the beam-based migration and LSM methods — Born data. (a-c) Images obtained by the migration operation of Tuvi et al. (2020b) for the full and sparse data sets. (d-f) Images obtained by the proposed LSM method for the full and sparse data sets. The full and sparse data set images resemble the true reflectivity. (g-i) Comparison over the line at x = 4.6 km.

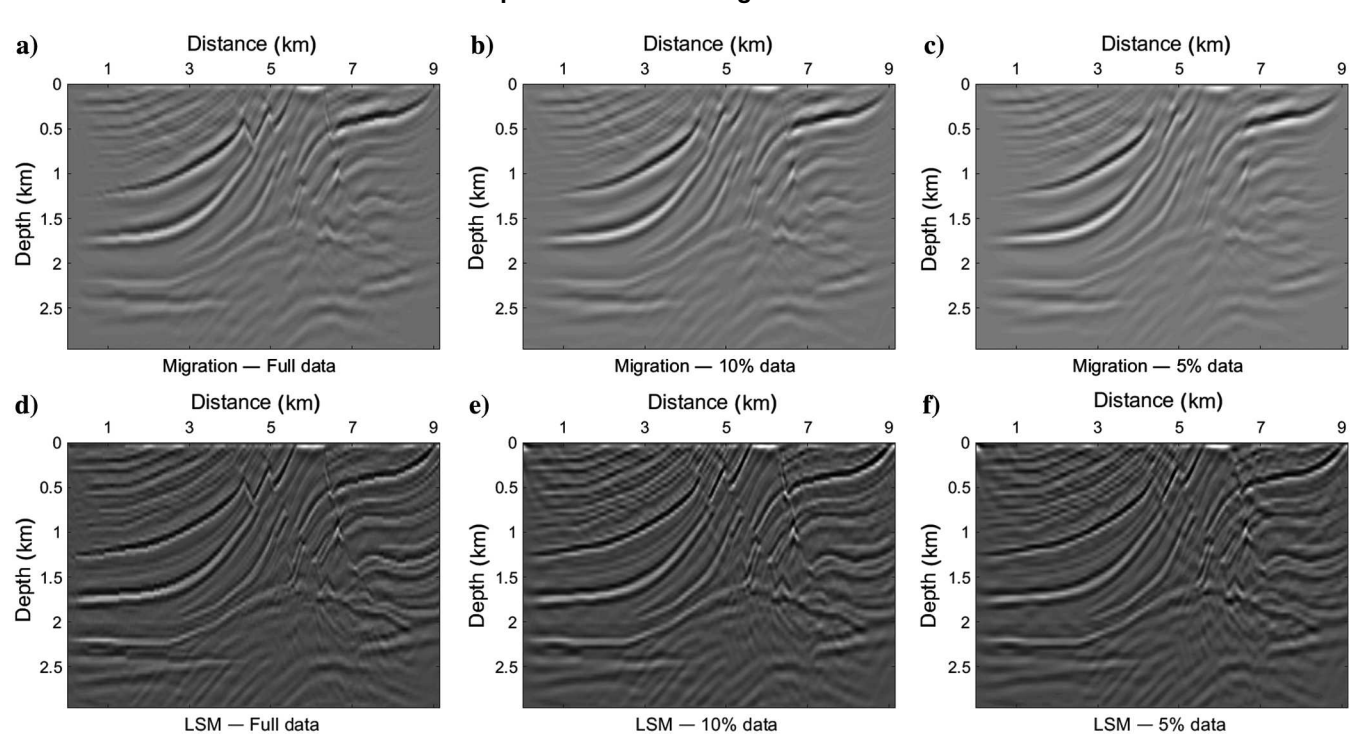


Figure 4. Image results obtained by the beam-based migration and LSM methods — full wavefield data. (a-c) Images obtained by the migration operation of Tuvi et al. (2020b) for the full and sparse data sets. (d-f) Images obtained by the proposed LSM method for the full and sparse data sets. The full and sparse data sets images resemble the true reflectivity.

CONCLUSION

This paper presents a new approach for image-domain LSM using a compressed data set. The method is based on the UWB-PS-BS method. Unlike GB methods, based on point source expansion as a summation of GBs, the UWB-PS-BS method is based on a frame decomposition for scattered data. This decomposition extracts significant scattering events (local Snell's law reflection) from original shot gathers. The phase space represents these subsurface physical properties using only a small number of elements. We use this unique property to extract only the relevant data (those with significant amplitude) to perform image-domain LSM. We demonstrate the advantages of our approach through numerical examples. We show good agreement between the full and sparse data set images. These results also demonstrate the efficiency of the proposed approach. We show that the proposed method is able to efficiently construct the Hessian, which enables the fast image-domain LSM implementation.

ACKNOWLEDGMENT

This work was partially supported by an NSF grant EAR 1723019.

DATA AND MATERIALS AVAILABILITY

Data associated with this research are available and can be obtained by contacting the corresponding author.

REFERENCES

Aoki, N., and G. T. Schuster, 2009, Fast least-squares migration with a de-blurring filter: Geophysics, 74, no. 6, WCA83–WCA93, doi: 10.1190/1

Červený, V., 1982, Expansion of a plane wave into Gaussian beams: Studia Geophysica et Geodaetica, 26, 120–131, doi: 10.1023/A:1024849811430. Claerbout, J. F., 1976, Fundamentals of geophysical data processing:

McGraw-Hill Book Co., Inc.
Dai, W., P. Fowler, and G. T. Schuster, 2012, Multi-source least-squares reverse time migration: Geophysical Prospecting, **60**, 681–695, doi: 10.1111/j.1365-2478.2012.01092.x.

Hill, N. R., 2001, Prestack Gaussian-beam depth migration: Geophysics, **66**, 1240–1250, doi: 10.1190/1.1487071.

Hu, H., Y. Liu, Y. Zheng, X. Liu, and H. Lu, 2016, Least-squares Gaussian beam migration: Geophysics, 81, no. 3, S87–S100, doi: 10.1190/ geo2015-0328.1.

Nemeth, T., C. Wu, and G. T. Schuster, 1999, Least-squares migration of incomplete reflection data: Geophysics, **64**, 208–221, doi: 10.1190/1

Pestana, R. C., and P. L. Stoffa, 2010, Time evolution of the wave equation using rapid expansion method: Geophysics, 75, no. 4, T121–T131, doi:

Plessix, R.-E., 2006, A review of the adjoint-state method for computing the gradient of a functional with geophysical applications: Geophysical Journal

International, 167, 495–503, doi: 10.1111/j.1365-246X.2006.02978.x. Schuster, G. T., 1993, Least-squares cross-well migration: 63rd Annual International Meeting, SEG, Expanded Abstracts, 110–113, doi: 10

Shlivinski, A., E. Heyman, A. Boag, and C. Letrou, 2004, A phase-space beam summation formulation for ultra wideband radiation: IEEE Transactions on Antennas and Propagation, 52, 2042–2056, doi: 10.1109/TAP.2004.832513.
 Tang, Y., 2009, Target-oriented wave-equation least-squares migration/in-

version with phase-encoded Hessian: Geophysics, 74, no. 6, WCA95-WCA107, doi: 10.1190/1.3204768.

Tarantola, A., 1984, Inversion of seismic reflection data in the acoustic approximation: Geophysics, 49, 1259–1266, doi: 10.1190/1.1441754.

Tuvi, R., Z. Zhao, and M. K. Sen, 2020a, A fast image domain least squares migration method with local data target approach: 90th Annual International Meeting, SEG, Expanded Abstracts, 2893–2897, doi: 10.1190/segam2020-3423961.1. A56 Tuvi et al.

Tuvi, R., Z. Zhao, and M. K. Sen, 2020b, Multifrequency beam-based migration in inhomogeneous media using windowed Fourier transform frames: Geophysical Journal International, 223, 1086–1099, doi: 10.1093/gji/ggaa365.

1093/gji/ggaa365.
Valenciano, A. A., B. Biondi, and A. Guitton, 2006, Target-oriented wave-equation inversion: Geophysics, 71, no. 4, A35–A38, doi: 10.1190/1.2213359.
Yu, J., J. Hu, G. T. Schuster, and R. Estill, 2006, Prestack migration deconvolution: Geophysics, 71, no. 2, S53–S62, doi: 10.1190/1.2187732

Yuan, M., J. Huang, W. Liao, and F. Jiang, 2017, Least-squares Gaussian beam migration: Journal of Geophysics and Engineering, 14, 184–196, doi: 10.1088/1742-2140/14/1/184.

Yue, Y., Y. Liu, and S. H. Gray, 2021, Accelerating least-squares Kirchhoff time migration using beam methodology: Geophysics, **86**, no. 3, S221–S234, doi: 10.1190/geo2020-0629.1.

Biographies and photographs of the authors are not available.